Kinetics of disorder-to-fcc phase transition via an intermediate bcc state

Yongsheng Liu, Huifen Nie,* and Rama Bansil†
Department of Physics, Boston University, Boston, Massachusetts 02215, USA

Milos Steinhart
Institute of Macromolecular Chemistry, Academy of Sciences of the Czech Republic, Heyrovsky Sq. 2, 162 06 Prague 6, Czech Republic

Joona Bang‡ and Timothy P. Lodge
Department of Chemical Engineering & Materials Science and Department of Chemistry, University of Minnesota, Minneapolis, Minnesota 55455, USA

(Received 7 November 2005; revised manuscript received 22 February 2006; published 29 June 2006)

Time-resolved small-angle x-ray scattering measurements reveal that a long-lived intermediate bcc state forms when a poly(styrene-*b*-isoprene) diblock copolymer solution in an isoprene selective solvent is rapidly cooled from the disordered micellar fluid at high temperature to an equilibrium fcc state. The kinetics of the epitaxial growth of the [111] fcc peak from the [110] bcc peak was obtained by fitting the scattering data to a simple model of the transformation. The growth of the [111] fcc peak agrees with the Avrami model of nucleation and growth kinetics with an exponent $n=1.4$, as does the initial decay of the [110] bcc peak, with an exponent $n=1.3$. The data were also found to be in good agreement with the Cahn model of grain boundary nucleation and growth.

DOI: 10.1103/PhysRevE.73.061803 PACS number(s): 61.41.+e, 64.60.My, 64.60.Qb, 61.10.Eq

I. INTRODUCTION

There has been considerable interest in the formation of a stable bcc crystal from a spherical liquid. Alexander and McTague (AM) suggested that for any spherical interaction potential the bcc state should be favored in freezing from the disordered state [1]. Simulations and experiments produced somewhat contradictory results with the AM condition. Recently Klein [2], following earlier work on deeply quenched liquids by Klein and Leyvraz [3], argued that the nucleated droplet is in the bcc phase, satisfying the AM condition, but it is unstable. A long-lived metastable bcc phase was found by Bang *et al.* [4] on heating a disordered micellar solution of poly(styrene-b-isoprene) (SI) diblock in squalane, a selective solvent for the polyisoprene (PI) blocks, from room temperature to the fcc phase around 70 °C. In this low temperature range a stable bcc phase is not observed. This SI block copolymer in tetradecane solution was extensively examined by Lodge's group and a stable bcc state was observed at higher temperatures, just below the disorder to order transition (DOT) [5]. On further cooling, the bcc state undergoes an order-order transition (OOT) to the fcc phase [5]. The presence of a stable bcc state between the disordered micellar fluid and the fcc state allows the possibility of examining whether an intermediate bcc phase nucleates first and subsequently transforms to the fcc state, or whether the fcc state nucleates directly from the liquid on rapid cooling. The bcc to fcc transformation has been shown to be an epitaxial transition in these block copolymer solutions [6,7]. Synchrotron based small-angle x-ray scattering (SAXS) measurements provide high wave-number (q) resolution and sufficiently high flux to follow the kinetics of the transition following a rapid temperature quench. In this paper we report the kinetics of the transition to the fcc phase by quenching a high temperature disordered micellar solution of the same SI diblock copolymer as used in Ref. [5] using tetradecane as the isoprene selective solvent.

II. EXPERIMENTAL SECTION

The symmetric SI diblock copolymer was synthesized by sequential living anionic polymerization [4,8,9], with molecular weights of 15 kg/mol for both PS and PI blocks, and polydispersity index of 1.02. The solvent tetradecane was used as received (Aldrich). A solution of volume fraction 15% was prepared gravimetrically. The phase behavior of this sample in tradecane has been reported in Ref. [5]. Time-resolved SAXS experiments were done at beamline X27C of the National Synchrotron Light Source (NSLS) of Brookhaven National Laboratory, using x-rays of wavelength $\lambda=0.1366$ nm (9.01 keV) with energy resolution $dE/E=1.1\%$. A two-dimensional charge-coupled device (CCD) detector with an 1024×1024 array was used to collect the scattering intensity. Azimuthal integration of the image was performed to obtain the scattering intensity $I(q)$ versus the scattering vector $q=(4\pi/\lambda)\sin\theta$, with 2θ being the scattering angle. The sample-to-detector distance of 1.957 m covers the range $0.1<q<2$ nm^{-1}. The q resolution was 4×10^{-3} nm^{-1}. Details of the experimental setup and data analysis are described in our previous work [10] on disorder

*Present address: Department of Biochemistry and Biophysics, University of North Carolina, Chapel Hill, NC 27599.
†Author to whom correspondence should be addressed. Email address: rb@bu.edu
‡Present address: Department of Chemical and Biological Engineering, Korea University, Seoul 136–713, Republic of Korea.

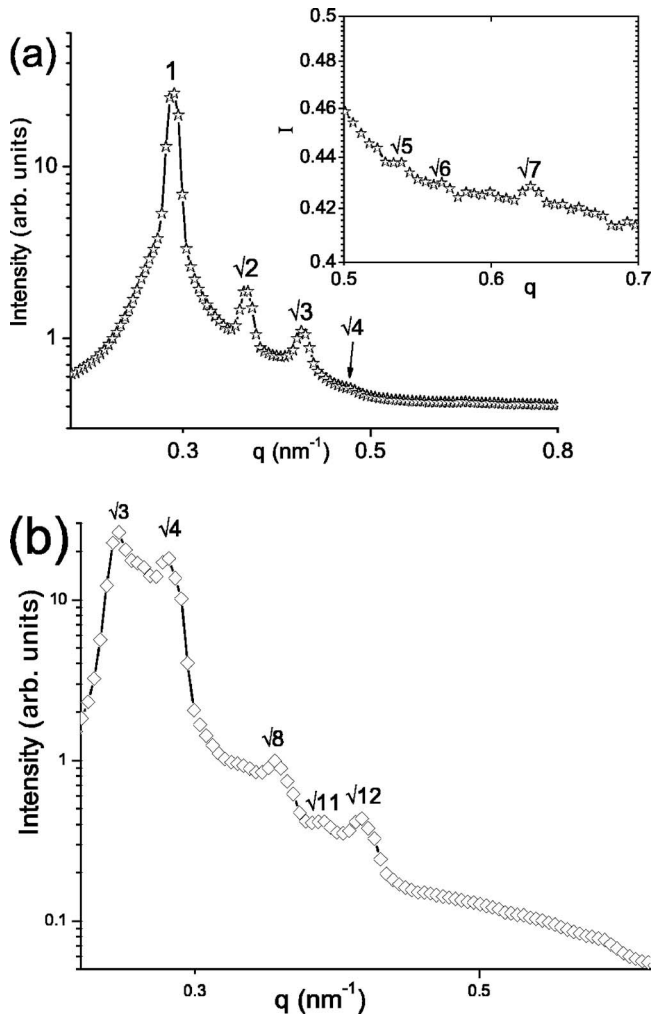

FIG. 1. SAXS data at (a) 80 °C and (b) 70 °C for SI (15-15) 15% in tetradecane. The inset in (a) shows the data at higher q at a higher magnification to reveal the higher order Bragg peaks characteristic of a bcc structure.

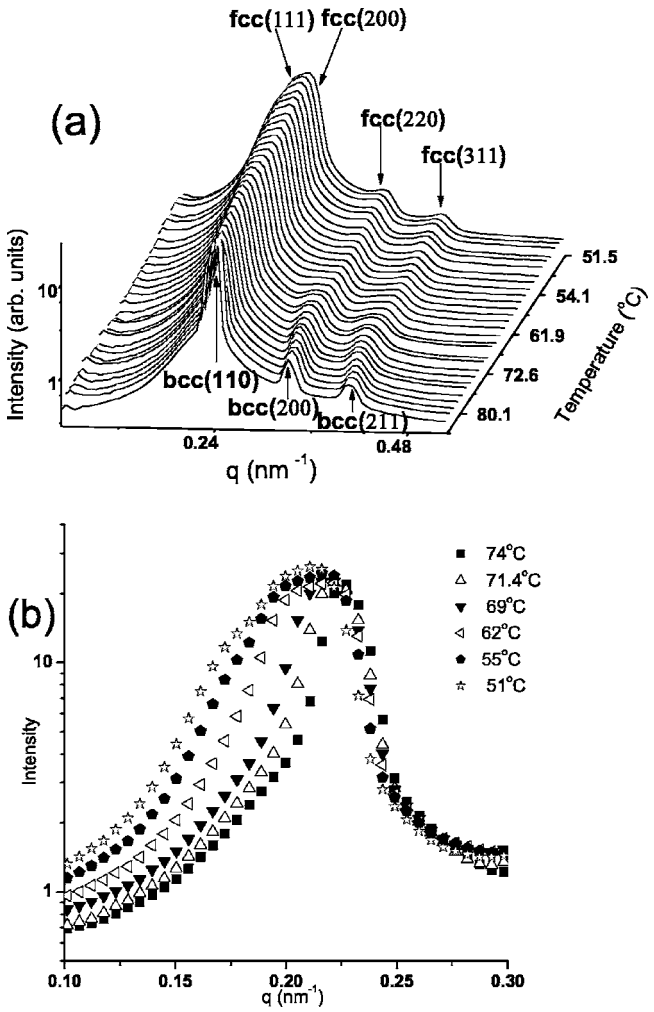

FIG. 2. (a) Time evolution of the SAXS intensity during a temperature ramp from 80 °C to 50 °C for SI solution in tetradecane. Initially, the sample was maintained at 80 °C for 10 min and the relative positions of the three peaks are consistent with the bcc peaks as indicated. As the sample was cooled down at a rate of 0.5 °C/min, changes in the scattering profile can be identified in the vicinity of 70 °C. The relative positions of the Bragg peaks are consistent with an fcc structure as indicated on the last frame at 50 °C. (b) A few frames of data in the vicinity of the primary peak are selected to show the transformation process more clearly and locate the OOT temperature around 70 °C.

to bcc kinetics in a triblock copolymer solution in a selective solvent. The sample was filled in a custom built cell with Kapton windows whose temperature was controlled by a Peltier module [10]. The time evolution of SAXS data was measured following either a temperature ramp or a temperature jump protocol. The former serves to locate the ODT, while the latter provides isothermal kinetics of the order-order transformation. In both the temperature ramp and jump measurements we recorded the scattering intensity $I(q)$ for 10 s per frame; data transfer from the two-dimensional (2D) CCD array took an additional 7 s/frame. The total duration of each run was 1.5 to 2 h.

III. RESULTS AND DISCUSSION

A. Confirmation of bcc and fcc structures and determination of the transition temperatures

SAXS data averaged for a long time (10 min) at 80 °C and 70 °C are shown in Fig. 1. Figure 1(a) shows the bcc structure at 80 °C up to the seventh order Bragg peak, which rules out simple cubic. The Bragg peaks in Fig. 1(b) confirm the fcc structure at 70 °C.

To identify the transition temperature we performed a temperature ramp from 80 °C to 50 °C at a cooling rate of 0.5 °C/min. As shown in Fig. 2(a), a change in the relative positions of the Bragg peaks is clearly visible. The data at 80 °C shows three peaks in the relative ratios of $\sqrt{1}:\sqrt{2}:\sqrt{3}$ which we take as an indication of a bcc structure. (The short averaging time for each frame in the ramp experiment leads to lower signal to noise; thus it is not possible to see higher order peaks in a ramp measurement.) The lower temperature structure with peaks at $\sqrt{3}:\sqrt{4}:\sqrt{8}:\sqrt{11}$ is indicative of an fcc structure. The order-order transition (OOT) from bcc to fcc occurs around 70 °C in agreement with the measured phase

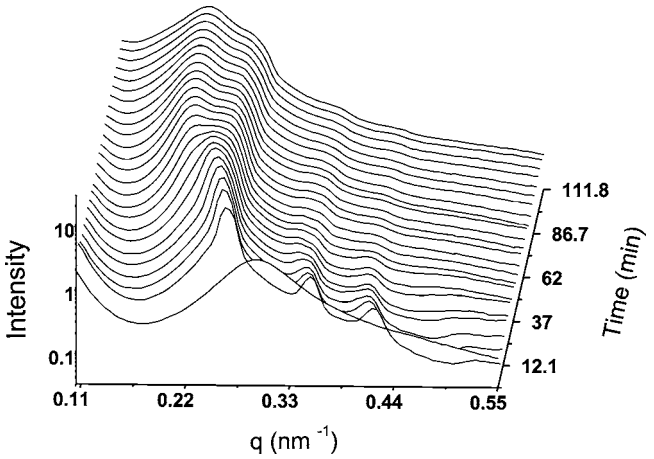

FIG. 3. Temperature jump measurements from 110 °C to 50 °C, showing the transition process of disordered to fcc via an intermediate bcc state.

diagram of SI in tetradecane [5]. The disorder to order transition occurs between 95 to 100 °C. As expected, the transition temperature measured in a ramp will be slightly higher than the ODT of 90 °C found in Ref. [5] which gives the equilibrium phase diagram, since in a ramp measurement the sample does not anneal at any temperature long enough for the phase to fully develop.

B. Kinetics of the transformation process

To follow the kinetics temperature jump (T jump) measurements were made by rapidly quenching the sample from 110 °C to 50 °C and 100 °C to 60 °C. Due to the slow rate of heat transfer in cooling the sample took 200–300 s to reach the final temperature.

Both the T-jump measurements starting from a disordered state to the fcc state showed qualitatively similar results. Figure 3 shows the time evolution of $I(q)$ for the T jump from 110 °C to 50 °C. An ordered phase with Bragg peak positions in the ratio $1:\sqrt{2}:\sqrt{3}$ characteristic of a bcc structure formed rather quickly, only 90 sec after the temperature changed, even before the temperature had reached the final value.

This intermediate state persisted well beyond the temperature equilibration time (less than 5 min). For the first 30 min the structure is purely bcc; the primary peak's intensity grows as shown in Fig. 4(a). Since the temperature had equilibrated in less than 5 min to 50 °C, where the stable phase is fcc, this long-lived bcc state is deeply supercooled. Around 45 min after the initial quench, a broad unresolved doublet becomes visible [see Fig. 4(b)] and at about an hour the doublet is clearly resolved into two peaks corresponding to the [111] fcc peak (0.16 nm^{-1}) and [110] bcc (0.21 nm^{-1}). The [111] fcc peak grows with time while the [110] bcc diminishes, implying that after 30 min the bcc phase transforms epitaxially to fcc [6,7] as shown in Fig. 4(b). The initial growth of the bcc from the disordered liquid is shown in Fig. 4(a). In this early time regime, the primary peak's position decreases, its intensity increases while the width decreases with time. These observations are qualitatively similar to those reported in previous studies of the growth of the bcc phase from a disordered micellar fluid in a styrene-ethylene-co-butylene triblock copolymer in mineral oil, a selective solvent for the EB block [10].

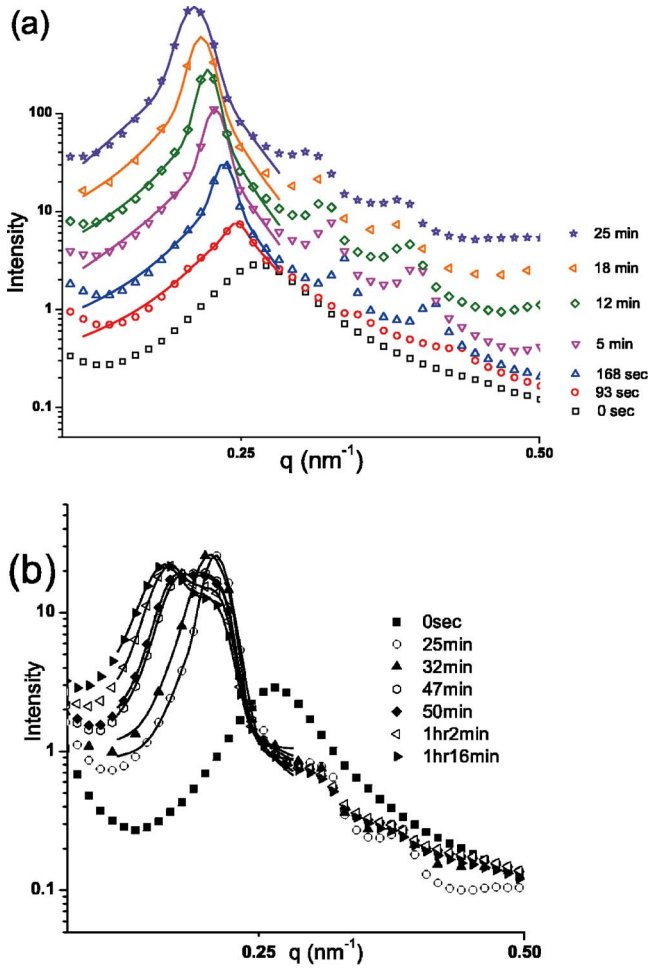

FIG. 4. (Color online) Time evolution of the SAXS intensity $I(q)$ following a temperature jump from 110 °C to 50 °C. (a) The early part showing an intermediate bcc state evolving from the disordered state shown at $t=0$. The data are shifted by a factor of 5 on the y axis to improve readability. (b) The later part showing the transition from bcc to fcc phase after 30 min. Solid lines are the fits to the data in the vicinity of the primary Bragg peaks, using the model described later in the text.

The time evolution of the intensity and position of the [110] bcc peak and [111] fcc peak shown in Fig. 5(a) reveals that the intensity of the [110] bcc peak increases while its position shifts to lower q at earlier time. At about 30 min, the [110] bcc peak intensity begins to decrease, while the [111] fcc peak first becomes noticeable at around 45 min. Although the transformation begins at around 30 min it does not go to completion during the 2-h run of our experiment. Bang *et al.* [4] observed that annealing of the fcc structure took longer than 4 h on heating SI in squalane from 25 °C to 65 °C. Our observation of a similarly slow transformation in a somewhat lower viscosity solvent is perhaps not surprising, especially since transitions are generally slower on cooling than heating.

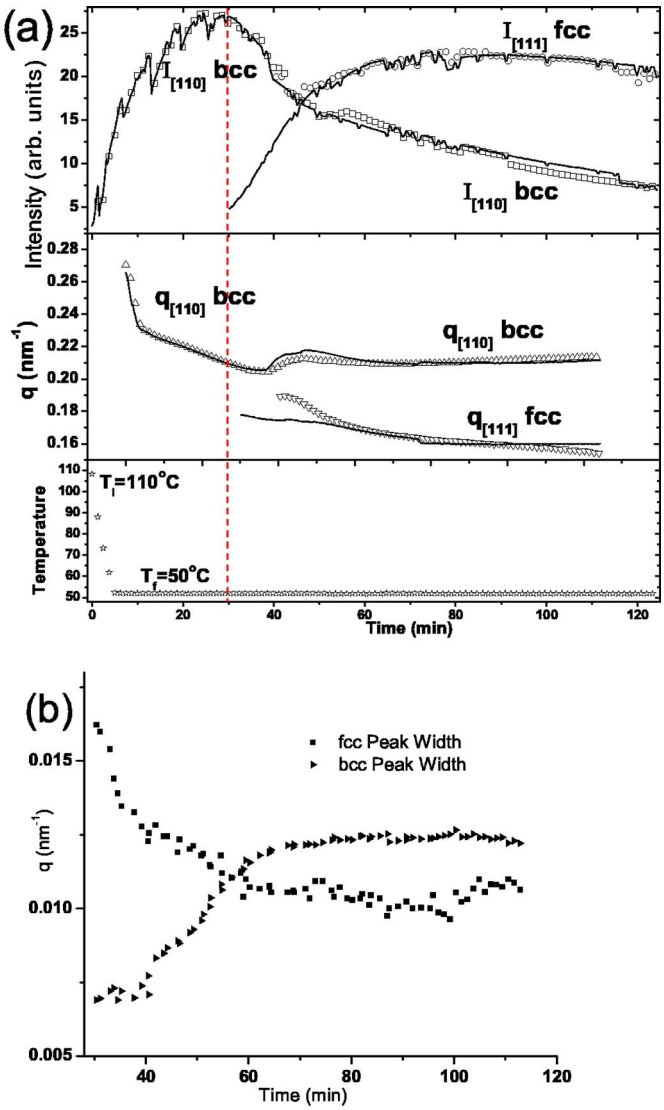

FIG. 5. (Color online) (a) Time evolution of intensity and position of [110] bcc peak and [111] fcc peak. Solid lines are fits of the model of transformation from bcc to fcc, as discussed in the text. This transformation occurs after 30 min as indicated by the dashed vertical line. The temperature (stars) equilibration following the quench from 110 °C to the final value of 50 °C is also shown. (b) Time evolution of the width of [111] fcc and [110] bcc peaks during the transformation process. Note that the zero of the time axis starts at 30 min.

C. Analysis of the *T*-jump data

To follow the kinetics of the bcc - fcc structural change, we fit the experimental data in the q range of the primary fcc and bcc peaks (0.1 – 0.3 nm^{-1}) using a simple model for the transformation. The scattered intensity $I(q)$ can be written as

$$I(q) = KP(q)S(q), \tag{1}$$

where $P(q)$ is the form factor, $S(q)$ is the structure factor, and K is a constant. For spherical micelles with radius R_c, the form factor $P(q)$ can be written as

$$P(q) = \nu_0^2 \phi^2(qR_c), \tag{2}$$

where $\nu_0 = 4/3\pi R_c^3$ is the volume of the sphere and

$$\phi(x) = \frac{3}{x^3}[\sin(x) - x\cos(x)]. \tag{3}$$

The structure factor $S(q)$ during the transformation is the addition of bcc and fcc contributions in proportion to the amount of transformed material. We modeled these as Gaussians centered at $q[111]$ and $q[110]$ for the fcc and bcc structures, respectively. Since the diblock micelles are in solution we also added a Lorentzian term to represent the liquidlike scattering. For each frame, the radius R_c was determined from the first minimum of the form factor, $qR_c = 4.49$, which was identifiable in the scattering data. We found that R_c increased from 8.5 nm at 110 °C to 11.5 nm at 50 °C during the transformation. These values of R_c are close to those reported for the same polymer in tetradecane (10 nm at 30 °C and 8 nm at 80 °C) [5]. The solid lines in Fig. 4(b) show the least squares fit to the scattering data with the positions, intensities and widths of the two Gaussians and the Lorentzian as fitting parameters. The typical reduced χ^2 of the fitting for each time frame is about 0.1.

Figure 5(a) shows the time dependence of the intensities and positions calculated in the fit, which agree very well with experimental data for both peak intensity and position. The width of the [110] bcc peak *increases* from 0.007 to 0.012 nm^{-1} with time, while that of the [111] fcc peak *decreases* from 0.016 to 0.01 nm^{-1}, as shown in Fig. 5(b). Changes in width reflect strain broadening effects as well as changes in grain size; larger grains produce narrower peaks. Although we have not done a detailed analysis of the different contributing factors, the width changes are qualitatively consistent with the expectation that fcc grains grow while bcc grains shrink.

D. Nucleation and growth kinetics

The kinetics of phase transformations in polymer and other systems has often been interpreted using the Mehl-Johnson-Avrami steady-state nucleation theory [11]. Assuming that the intensities are proportional to the amount of the transformed material, we use the Avrami [11–15] model to describe the growth of the fcc phase from the bcc state,

$$I(t) - I(t_0) = [I(t_\infty) - I(t_0)](1 - e^{-k(t-t_0)^n}). \tag{4}$$

Here t_0, the time at which the transformation from bcc to fcc becomes apparent, is taken as 30 min. The transformation rate k and the Avrami exponent n were determined by fitting Eq. (4) to the peak intensity data shown in Fig. 6. The results indicate that $n = 1.4$ is in reasonable agreement with the data for T jump from 110 °C to 50 °C. Similar agreement, with $n = 1.55$, was obtained for the data from the other T jump from 100 °C to 60 °C. If we restrict ourselves to the early part of the bcc → fcc transformation then the decay of the bcc state

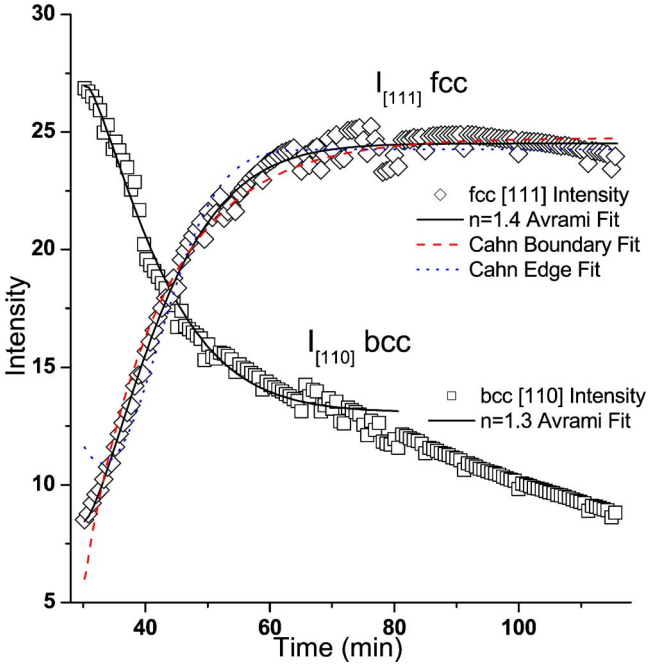

FIG. 6. (Color online) Calculation of the [111] fcc and [110] bcc peak intensity using different models for kinetics of nucleation and growth as discussed in the text: Avrami model (solid line), Cahn model for grain boundary (dashed line), and grain edge (dash-dot line).

$$I(t) - I(t_\infty) = [I(t_0) - I(t_\infty)]e^{-k(t-t_0)^n}. \tag{5}$$

fits well with Eq. (5) with $n=1.3$, suggesting that both the growth of the fcc phase and the initial decay of the bcc phase follow the same mechanism, as expected for a transformation process. This is further supported by the similarity of the rate of transformation: $k^{1/n}$ equals 0.072 s^{-1} for the fcc growth and 0.073 s^{-1} for the bcc decay. We note that the fit to the bcc intensity breaks down at late times, perhaps due to the difficulty of determining the bcc peak intensity at late times because it is very weak and its position is in between the fcc doublet.

The exponent n has been used as an indicator of the geometry of the growing crystal in the polymer crystallization literature [12] as well as for order-order transitions in block copolymers [16]. It has also been used to characterize the nature of the nucleation and growth process for polymorphic changes from one lattice to another [11]. Under conditions when all nucleation sites are saturated in the beginning, the exponent depends on the spatial dimensionality d of the interface on which growth occurs as $n=3-d$. If growth occurs on the boundary surface between two grains (referred to as grain boundary nucleation and growth) then $d=2$ and $n=1$, whereas if the growth occurs on an edge between three adjacent grains then $d=1$ and $n=2$.

Cahn [17] developed a model to describe heterogeneous nucleation on defects such as grain boundaries, grain edges or grain corners. The Cahn model for growth on grain boundaries has been shown to agree very well with time-resolved SAXS data on the initial stages of ordering kinetics of polystyrene-polybutadiene diblock copolymer solutions following a temperature quench from the disordered state [18,19]. In the following we present an analysis of our data using the model obtained by Cahn for grain boundary and grain edge nucleation and growth, according to which

$$I(t) - I(t_0) = [I(t_\infty) - I(t_0)](1 - e^{-b_s f_s(a_s t)}), \tag{6}$$

where $a_s=(I_s G^2)^{1/3}$, $b_s=\left(\frac{I_s}{8S^3G}\right)^{-1/3}$ and

$$f_s(a_s t) = a_s t \int_0^1 (1 - e^{-\pi(a_s t)^3[(1-x^3)x^2(1-x)]/3})dx \tag{7}$$

Here I_s denotes the nucleation rate per unit boundary surface area, G is the growth rate on the grain boundary surface, and S is the boundary surface area per unit volume. With this notation, a_s has the unit of s^{-1}, while b_s is dimensionless. Using similar notation for nucleation and growth on the grain edge of length L,

$$I(t) - I(t_0) = [I(t_\infty) - I(t_0)](1 - e^{-b_s f_s(a_s t)}) \tag{8}$$

where $a_e=(I_e G)^{1/2}$, $b_e=\left(\frac{I_e}{2\pi GL}\right)^{-1}$ and

$$f_e(a_e t) = (a_e t)^2 \int_0^1 x(1 - e^{-(a_e t)^2[(1-x^2)^{1/2} - x^2 \ln((1+\sqrt{1-x^2})/x)]})dx. \tag{9}$$

We fit the peak intensity data of Fig. 5(a) to the equations above. The results are shown in Fig. 6 with the parameters for the best fits as $I_s/S=5.2$ s^{-1} nm^{-1} and $GS=6.9\times10^{-4}$ s^{-1} for the grain boundary model and $I_e/L^{1/2}=9.16$ s^{-1} and $GL^{1/2}=7.10\times10^{-4}$ s^{-1} for the grain edge model. The grain boundary calculation (reduced $\chi^2=2.07$) appears to fit somewhat better than the grain edge model (reduced $\chi^2=3.18$). However, as is clear from Fig. 6, the Avrami equation with the value $n=1.4$, which lies between the predictions of $n=1$ for nucleation and growth on the boundary surface and 2 for grain edge nucleation after saturation, fits the data the best.

The calculations with the grain boundary model allow us to estimate the nucleation rate I_s and the growth rate G from the parameters of the fitted functions for the grain boundary model ($I_s/S=5.2$ s^{-1} nm^{-1} and $GS=6.9\times10^{-4}$ s^{-1}) if we know S. For a grain of diameter D, $S\sim1/D$ [17] with a proportionality constant which depends on the shape of the grain. An estimate of D can be obtained from the width w of the Bragg peak, $D\approx2\pi/w\approx630$ nm, using $w\approx0.01$ nm^{-1} [see Fig. 5(b)]. Since the nearest neighbor distance $d\approx2\pi/q_{[111]}\approx30$ nm the characteristic time scale for one crystallite to grow a distance comparable to the nearest neighbor separation of micelles is in the range of 1–2 min.

IV. CONCLUSIONS

In conclusion, we note that a long-lived intermediate bcc state appears when disordered micelles of a SI diblock copolymer in a selective solvent are rapidly quenched to the fcc state. After some time, this bcc state transforms slowly to the fcc phase. Although the sample crosses the stable bcc phase

boundary as it is cooled from the disordered fluid, the time that it spends in crossing the bcc phase is much smaller than the duration of the intermediate bcc state and the first appearance of the fcc structure. This suggests that the bcc state nucleates first and later transforms to fcc, rather than a direct nucleation of the fcc state. The time evolution of the growth of intensity of the [111] fcc peak agrees with the Avrami model, with an exponent $n=1.4$, intermediate between that predicted for grain boundary nucleation and grain edge nucleation after saturation. The decay of the [110] bcc intensity also follows the Avrami model with $n=1.3$. We found that the Cahn model of grain boundary nucleation and growth fits slightly better than that for nucleation and growth on edges.

ACKNOWLEDGMENTS

This research was carried out at NSLS, Brookhaven National Laboratory, which is supported by the U.S. Department of Energy, Division of Materials Sciences and Division of Chemical Sciences, under Contract No. DE-AC02-98CH10886. We thank Professor Ben Chu and Professor Ben Hsiao, and Dr. Igor Sics and Dr. Lixia Rong for their support at beamline X27C of NSLS. R.B. acknowledges the support of NSF Division of Materials Research (NSF-DMR Grant No. 0405628). T. P. L and J. B. acknowledge support from the National Science Foundation through the University of Minnesota MRSEC (Grant No. DMR-0212302).

[1] S. Alexander and J. McTague, Phys. Rev. Lett. **41**, 702 (1978).
[2] W. Klein, Phys. Rev. E **64**, 056110 (2001).
[3] W. Klein and F. Leyvraz, Phys. Rev. Lett. **57**, 2845 (1986).
[4] J. Bang and T. P. Lodge, Phys. Rev. Lett. **93**, 245701 (2004).
[5] J. Bang, K. Viswanathan, T. P. Lodge, M. J. Park, and K. Char, J. Chem. Phys. **121**, 11489 (2004).
[6] J. Bang, T. P. Lodge, X. Wang, K. L. Brinker, and W. R. Burghardt, Phys. Rev. Lett. **89**, 215505 (2002).
[7] M. J. Park, J. Bang, T. Harada, K. Char, and T. P. Lodge, Macromolecules **37**, 9064 (2004).
[8] K. J. Hanley, T. P. Lodge, and C. I. Huang, Macromolecules **33**, 5918 (2000).
[9] T. P. Lodge, B. Pudil, and K. J. Hanley, Macromolecules **35**, 4707 (2002).
[10] H. Nie, R. Bansil, K. Ludwig, M. Steinhart, C. Konak, and J. Bang, Macromolecules **36**, 8097 (2003).
[11] R. W. Cahn and J. W. Christian, *Physical Metallurgy* (North-Holland, Amsterdam, 1965), p. 486.
[12] J. M. Schultz, *Polymer Crystallization* (Oxford University Press, New York, 2001), p. 180.
[13] M. Avrami, J. Chem. Phys. **7**, 1103 (1939).
[14] M. Avrami, J. Chem. Phys. **8**, 212 (1940).
[15] M. Avrami, J. Chem. Phys. **9**, 177 (1941).
[16] G. Floudas, R. Ulrich, U. Wiesner, and B. Chu, Europhys. Lett. **50**, 182 (2000).
[17] J. W. Cahn, Acta Metall. **4**, 449 (1956).
[18] C. R. Harkless, M. A. Singh, S. E. Nagler, G. B. Stephenson, and J. L. Jordan-Sweet, Phys. Rev. Lett. **64**, 2285 (1990).
[19] M. A. Singh, C. R. Harkless, S. E. Nagler, R. F. Shannon Jr., and S. S. Ghosh, Phys. Rev. B **47**, 8425 (1993).